PFC/JA-82-12

IMPURITY INJECTION EXPERIMENTS ON THE ALCATOR C TOKAMAK

E. S. Marmar, J. E. Rice, J. L. Terry
Plasma Fusion Center
Massachusetts Institute of Technology
Cambridge, MA 02139

F. H. Seguin
American Science and Engineering
Cambridge, MA 02139

June 1982

This work was supported by the U.S. Department of Energy Contracts DE-AC02-78ET51013 and DE-AC02-77ET53068. Reproduction, translation, publication, use and disposal, in whole or in part by or for the United States government is permitted.

IMPURITY INJECTION EXPERIMENTS ON THE ALCATOR C TOKAMAK

E. S. Marmar, J. E. Rice, J. L. Terry

Plasma Fusion Center
Massachusetts Institute of Technology
Cambridge, MA 02139

F. H. Seguin

American Science and Engineering
Cambridge, MA 02139

ABSTRACT

Transport of trace, non-recycling, injected impurities has been studied on the Alcator C tokamak. Changes of impurity confinement times with varying plasma density, current, toroidal field, majority ion species mass, impurity charge and mass, Z_{eff}, and major and minor radius have been delineated. An empirical scaling is developed from these results and compared with the results of similar transport studies undertaken on other tokamak devices. The agreement is reasonable. A computer model simulating the transport is utilized to compare several models with the empirical results. With the possible exception of low density, high Z_{eff} discharges, the transport is not consistent with the predictions of neoclassical theory, but can be well described by simple spreading diffusion with a diffusion coefficient ranging from 1 to 5 x 10^3 cm^2/sec, depending on plasma parameters. This model yields good agreement both with the time histories of single chord measurements of various ionization states, and with radial soft X-ray emission profiles. Increased impurity transport with the onset of strong MHD oscillations has also been observed, with the effective diffusion coefficient scaling approximately as $(\Delta B)^4$.

1. Introduction

Impurities play an important role in determining the characteristics of all tokamak fusion plasmas. Through enhanced radiation, resistivity, thermal conduction and charge exchange, they can directly and adversely affect the energy balance of such plasmas, and for fixed electron density and plasma pressure, can significantly decrease the density of the reacting working gas ions. Energy loss due to impurity effects can completely dominate other loss mechanisms, leading in some cases[1] to hollow temperature profiles and very poor global energy confinement times. In order to understand the effects that impurities can produce in presently operating devices, and to predict their behavior in future, higher power, longer pulse experiments, it is important to study the mechanisms responsible for impurity generation at the limiters and walls and to study the subsequent transport of the impurities after they penetrate the edge plasma. It is this latter concern which is addressed in this paper.

Trace impurities have been injected into Alcator C plasmas[2] in order to study their transport properties. Similar experiments have been performed in ATC[3], Alcator A[4], TFR[5], ISX-B[6], FT-1[7], PDX[8] and PLT[9]. In Alcator C, aluminum, silicon, titanium and molybdenum have been introduced by the laser blow-off technique[10], and nitrogen and argon have been been injected through a pulsed gas valve. Subsequent emissions from the various charge states have been monitored with a variety of instruments: a 1/8 m. normal incidence VUV monochromator (1200 Å $< \lambda <$ 2300 Å), a 1 m. grazing incidence monochromator (40 Å $< \lambda <$ 550 Å), a flat crystal spectrometer with a PET crystal (1 Å $< \lambda <$ 8 Å) and an X-ray diode imaging array ($h\nu \gtrsim$ 1.5 keV). The ultimate time resolution of the spectrometers

is ~ 100 μs and the line of sight spatial resolution of all detectors is ~ 1 cm. A parameter study of injections has been performed in H_2, D_2 and ^4He working gases by varying the plasma current ($100\ kA < I_p < 700\ kA$), the electron density ($5 \times 10^{13}\ cm^{-3} < n_e < 6.8 \times 10^{14}\ cm^{-3}$), the toroidal magnetic field ($35\ kG < B_T < 120\ kG$) and Z_{eff} ($1 < Z_{eff} < 3$). Experiments have been performed in plasmas with molybdenum limiters of radii 10, 16 and 16.5 cm, and the major radius has been varied between 57 and 71 cm with the 10 cm limiter.

2. Injection Technique Comparison

Before describing the results of the Alcator C impurity transport experiments, it is useful to compare the two most commonly used techniques of impurity injection (laser blowoff and gas puffing) and to discuss their propriety for transport studies. Fig. 1 shows the differences in impurity behavior when (a) a 1μ thick film of Si was blown off of a glass slide, and (b) a mixture of N_2 and Ar was puffed through a fast valve into the edge region of the discharge. Although the impurities were injected into similar discharges, the resulting impurity behaviors were qualitatively different. The time history of the source for impurities passing through the puffing valve is shown in the bottom trace of Fig. 1(b), while the source time history for the blown-off impurity may, for present purposes, be taken to be the Si^{3+} (1394 Å) time history in Fig. 1(a). (Note: The Si^{3+} was observed at the same toroidal location as that of the injector.) The characteristic influx times are ~20 ms and ~2 ms respectively. It is clear from Fig. 1 that the puffed N^{5+} (1897 Å) and Ar^{16+} (3.95 Å) remained in the plasma for the duration of the discharge ($\gtrsim$ 150 ms after the valve was closed), while the silicon left the plasma completely

in less than 50 ms. This behavior cannot be ascribed to the differences in source duration, nor can it be explained by differences in mass or charge of the injected impurities since the silicon has a charge and mass intermediate to those of nitrogen and argon. These effects are most reasonably explained by differences in recycling; the Si does not recycle, whereas the puffed gaseous impurities do. This is confirmed by observations of edge emissions from N^{4+} (1239 Å).

The characteristic duration of the source for gaseous impurities, when recycling is included, is clearly much longer than the ~ 20 ms during which the impurities were actually passing through the valve. Because of this recycling, the source time history is not well known, and this is an obvious disadvantage when studying the penetration of impurities and their subsequent loss. Similar problems are encountered when using intrinsic impurities to perform transport studies[11,12]. If, however, impurities need to be injected simply to seed the plasma (for impurity line broadening studies, for example), the gas puff method can be superior since large amounts can be introduced and since the recycling maintains the impurity level. In order to avoid these problems, all of the following transport results have been obtained using the laser blowoff technique for injection.

3. Injection Time Histories and Spatial Profiles

A typical discharge into which silicon was injected is depicted in Fig. 2. During the steady state portion of this 80 kG, H_2 discharge, the plasma current was 470 kA, the line averaged electron density was 2.8×10^{14} cm^{-3}, and the central electron temperature was 1200 eV. For this particular discharge, the limiter radius was 16 cm, the major radius was

64 cm and the limiter safety factor (q_L) was 3.4. Note the rapid increase in the Si^{10+} (303 Å) and Si^{13+} (6.18 Å) signals after the injection, followed by a more gradual decay. An estimate of the concentration of silicon at the center of the plasma, obtained by taking the ratio of the peak Si^{13+} emission to the off-line continuum X-ray emission, is $\sim 2 \times 10^{10}$ cm^{-3}. This is not enough to disturb the central plasma via radiation losses, as confirmed by the absence of significant effects of the injection on macroscopic plasma parameters such as the loop voltage, electron density and temperature, Z_{eff}, current, and total radiated power as measured bolometrically.

A more detailed look at specific Si emission lines during a sequence of similar deuterium discharges (B_T = 60 kG, I = 385 kA, $\bar{n}_e = 3.6 \times 10^{14}$ cm^{-3}, T_e = 1100 eV, and q_L = 3.13) is provided in Fig. 3, where the normalized chordal brightnesses of sodium-, beryllium-, helium-, and hydrogen-like silicon, as well as the central chord soft X-ray brightness are shown after the injection. The background emissions have been subtracted off. The peaks of the emissions occur sequentially in time as the silicon is ionized and transported to the plasma center. Each of the signals then decays to its pre-injection level, indicating that the silicon is leaving the plasma on a time scale shorter than the discharge length, with little or no recycling.

The spatial distribution of silicon emissions can be followed as a function of time with the broadband soft X-ray imaging system, which is sensitive primarily to the 1s-2p transitions of the helium- and hydrogen-like states. Figure 4 illustrates abel-inverted soft X-ray impurity radiation profiles obtained at various times after injection of silicon

into an H_2 discharge similar to that of Figure 2. This is only the component of X-radiation due to the injected silicon; the background continuum and line radiation has been subtracted off. Note the shell structure of the emission at early times as the silicon is being ionized and transported to the center. By 9 ms, the emission profile is peaked on axis and subsequently decays, more or less maintaining its shape.

4. Transport Models

These types of observations have been compared to the predictions of a 1-D impurity transport code[13] in an effort to understand the impurity transport mechanism in Alcator C. Assuming cylindrical symmetry, the code solves the coupled equations

$$\frac{\partial n_j}{\partial t} = -\frac{1}{r}\frac{\partial}{\partial r}(r\Gamma_j) + n_e\left[S_{j-1}\, n_{j-1} - S_j\, n_j + \alpha_j n_{j+1} - \alpha_{j-1}\, n_j\right]$$

$$j = 1, \ldots, Z \qquad (1)$$

where n_j is the density of the j^{th} ionization state, Γ_j is the flux, S_j is the ionization rate, and α_j is the recombination (radiative and dielectronic) rate.

The code predictions for the data of Figure 3, when the impurity flux is taken to have the neoclassical form[14]

$$\Gamma_j^{NC} = \rho_b^2\, \nu_{bj}\, \frac{Z_b}{Z_j}\, \frac{[1 + \gamma q^2]}{T_b}\left[T_b \frac{\partial n_b}{\partial r} - \frac{n_b}{n_j}\frac{Z_b T_j}{Z_j}\frac{\partial n_j}{\partial r} - \frac{Z_b n_b}{Z_j}\frac{\partial T_j}{\partial r}\right] \qquad (2)$$

(b denotes the background ion species), are shown in Figure 5. q is the safety factor, ρ is the ion gyroradius, ν is the ion-impurity collision frequency $\left(\frac{4}{3} \sqrt{2\pi}\ n_j Z_j^2 Z_b^2 e^4 \ln\Lambda/\sqrt{m_b}\ T_b^{3/2} \right)$, and γ is of order unity for trace impurities. Qualitative disagreement with the data is apparent, as the influx is too slow and the impurities are predicted to remain at the center of the plasma for a much longer time. This indicates that the neoclassical transport mechanism is replaced or supplemented by an anomalous mechanism. Two possibilities have been investigated for the functional form of the impurity flux:

$$\Gamma_j = - d \frac{\partial n_j}{\partial r} \tag{3}$$

$$\Gamma_j = \Gamma_j^{NC} - D \frac{\partial n_j}{\partial r} \tag{4}$$

The coefficients d and D could be arbitrary functions of position in the plasma, but here only the cases in which d is spatially constant and D has the radial dependence of the neoclassical coefficient of the $\frac{\partial n_j}{\partial r}$ term in the neoclassical flux (Eq. 2) were considered. Both forms for the flux can lead to predictions in which the impurities eventually leave the plasma with an exponential time dependence. With the appropriate choice of d or D, either model can provide good quantitative agreement with the data. For example, the code predictions for the observed emissions, with $d = 2.6 \times 10^3$ cm^2/sec, are shown in Fig. 6, and the agreement with the observations is shown in Fig. 3. The code prediction for the X-ray diode signal is calculated by adding the predicted brightnesses of the $\Delta n = 1$ transitions to the ground state in helium- and hydrogen-like

silicon.

Fig. 7 shows the time evolution of the uninverted brightness profiles of the silicon X-ray emission, as observed by the diode array, for a discharge from the series shown in Fig. 3. The solid curves in Fig. 7 are the appropriate profiles predicted by the code when the flux is again given by Eq. 3 with $d = 2.6 \times 10^3$ cm^2 sec^{-1}. In this case the agreement is also excellent.

Because the anomalous flux is so large relative to the neoclassical flux, neither the time histories of the line emissions nor the spatial evolution of the X-ray emission allow discrimination between the two forms for the flux (Eqs. 3 and 4). The variation of the anomalous diffusion coefficient with plasma parameters is discussed in Section 5.

The effects of sawteeth have been ignored in this analysis. It has been shown[15] that, while internal disruptions do cause observable, rapid spatial redistributions of impurity species near the plasma center (especially during the inflow stage, when the impurity density distribution is hollow), theoretical modeling indicates that sawteeth should not have a large effect on the gross time scales for either inflow or loss in the Alcator C discharges studied here.

5. Impurity Confinement Time Scalings

The model of Eq. 3 predicts an exponential decay for the emissions from the centrally located ionization states shortly after the peaks. The decay time constant, τ, is related to the diffusion coefficient, d, by $\tau = \frac{a^2}{k^2 d}$, where $k \equiv 2.405$ is the first zero of the zeroth order

Bessel function and a is the minor radius.

The falling signal of Si^{12+} in Fig. 3 is well described by an exponential and yields a decay time of 19 ms. Fits are typically taken between the times when the signal has fallen to 80% and to 10% of the peak value. This characteristic time is interpreted as the global particle confinement time for non-recycling injected trace impurities.

Fig. 8 shows the silicon confinement time, τ_{Si}, as a function of average electron density (at constant limiter q value) for hydrogen and deuterium discharges. τ_{Si} is a factor of 2 longer in deuterium than in hydrogen, and it is independent of electron density over the range shown. This independence does not pertain outside this density range. At the highest densities obtainable at a particular magnetic field, the confinement times are somewhat shorter. This decrease of impurity confinement time is not believed to be due to a direct density dependence per se, but rather to the increase in $m = 2$ and $m = 3$ MHD activity which is observed at the highest densities at a given magnetic field[16]. This is borne out by the observation that the thresholds for both MHD activity and impurity confinement deterioration occur at a higher density when the field is increased from 60 to 80 kG. The degradation of impurity confinement with an increasing level of MHD activity is shown by the upper points in Fig. 9. These data are from injections of aluminum into ^4He plasmas, where the normal confinement times are a factor of 4 longer than for similar hydrogen discharges.

The situation is different at the lower densities; below $\bar{n}_e \sim 2 \times 10^{14}$ cm^{-3}, the impurity confinement times dramatically increase and in some cases impurity accumulation is seen to occur, reminiscent of the neoclassi-

cal case (Fig. 5). However, at these same low densities, the Z_{eff} of the plasma also increases rapidly with decreasing density. (Large Z_{eff} values may explain the observations in Ref. 6.) In the Alcator C case, the increase in Z_{eff} has been attributed to a large molybdenum concentration at the low electron densities. Another condition that sometimes develops at low densities is an absence of sawtooth oscillations in the soft X-ray emission, which occurs when there are hollow temperature profiles[17] and large amounts of radiated[18] power. In any event, when Z_{eff} increases, the impurity confinement times increase as shown in Fig 10. It has not been determined whether the increase in trace impurity confinement is a result of larger Z_{eff} values, or if certain plasmas have a propensity for impurity confinement (hence a higher Z_{eff}) due to changes in other parameters.

The dependence of impurity confinement on limiter safety factor is exhibited in Fig. 11, where the impurity confinement times for aluminum, silicon and titanium are plotted against $1/q_L$ for hydrogen, deuterium and helium discharges. The increase of impurity confinement time with plasma current and with mass of the background ion is the same as was observed in Alcator A[4]. In addition, Fig. 11 includes data from a wide range of toroidal fields (30 kG < B_t < 120 kG). Since the confinement time decreases with increasing toroidal field, q_L^{-1} seems to be the relevant parameter. The slopes of the three lines are in the ratio 4:2:1, indicating a linear dependence on the mass of the background ion. Note that the data points from the different injected materials are intermixed. This is emphasized in Fig. 12, where the impurity confinement times (averaged over many shots) are plotted versus the charge of the injected impurity, at constant electron density and q_L in hydrogen. The points, in

increasing charge (with the wavelengths of the observed emissions), are from helium- (7.76 Å) and hydrogen- (7.17 Å) like aluminum, helium (6.65 Å) and hydrogen- (6.18 Å) like silicon, and beryllium- (169 Å) and helium- (2.62 Å) like titanium. There is no dependence on impurity charge or impurity ionization potential, at least for these central ions. A similar plot could have been produced as a function of impurity mass, again with no dependence. It should be noted that the charge to mass ratio of all these ions is about the same (.38 to .46), so that a dependence on charge to mass ratio cannot be ruled out.

Consider again the deuterium discharge of Fig. 3, where q_L was 3.1 and the silicon confinement time was 19 ms. This value is considerably longer than 13 ms or so for a similar discharge in Alcator C, with the 10 cm limiter. (q_L = 3.1 in deuterium, B_T = 80 kG, I_p = 200 kA, a_L = 10 cm, R = 64 cm.) This difference is believed to be attributable mainly to the change in minor radius. In Fig. 13 the silicon confinement time is shown as a function of limiter radius for hydrogen and deuterium discharges in Alcator C and Alcator A, at constant q_L. The data are consistent with a linear dependence on minor radius. This conclusion relies on the choice of what is to be held fixed (in this case q_L) when comparing plasmas of different minor radii.

It is also useful to determine the dependence of impurity confinement on the major radius of the machine. Operation of Alcator C with a 10 cm limiter at three major radii (57, 64 and 71 cm), has provided an indication of the dependence on R. The silicon confinement time (averaged over many injections) as a function of major radius at constant q_L for hydrogen and deuterium is shown in Fig. 14. The dependence is best described as

somewhere between R and $R^{1/2}$ but, within experimental errors, the data are also consistent with no dependence of τ_I on major radius.

Summarizing the scalings of this section, the impurity confinement time may be described as

$$\tau_I(ms) = \frac{.075\ a_L\ m_{bg}}{q_L}\ R^{.75}\ \frac{Z_{eff}}{Z_{bg}} \qquad (5)$$

with R and a_L in cm, m_{bg} in amu and where Z_{bg} is the charge of the background ion. For the centrally located ionization states, τ_I is independent of the charge and mass of the impurity, and the electron density (provided there is little or no MHD activity). In Fig. 15, the observed impurity confinement times are compared with those predicted by Eq. 5. 90% of the points are within 30% of the value predicted by Eq. 5. Note that the dependences on major radius and Z_{eff} should not be interpreted too literally, since certain other scalings would be in equally good agreement with the data. It is, however, well established empirically from these results that τ_I is approximately proportional to $a_L\ m_{bg}\ q_L^{-1}$.

The scalings of Eq. 5 may be compared with the results of impurity injection experiments on other tokamaks. Shown in Fig. 16 are data from injections into FT-1[7], PDX[8], TFR[5], ISX-B[6], and Alcator A[4], along with the lines from Fig. 15. Impurity confinement times in all these cases agree remarkably well, except for the TFR confinement times, which are all about a factor of two longer than predicted by Eq. 5. The ISX-B datum actually represents a lower limit, since in this case the decay time was significantly longer than the steady state portion of the plasma after the injection.

6. Discussion

Measurement of a single quantity (confinement time of a central impurity) cannot be expected to elucidate all of the details of the microscopic transport. The diffusion coefficient and its dependences, implied by the confinement time measurements, probably represent the overall effect of a number of transport mechanisms. For example, there may be inward convective terms which are dominated by larger diffusive terms to give a confinement time consistent with that predicted by $\Gamma_j = - d\, \partial n_j/\partial r$. Measurements of the density profiles of three successive ionization states for a well known source, or measurements of the total density profile of a given impurity, could be used to distinguish between the two possibilities. Where such measurements have been attempted[13,19] evidence for an inward convective term has been observed.

If there are a number of transport mechanisms, they probably respond in different ways to changes in plasma parameters. If the dominant mechanisms are diffusive, and if each is represented by a different diffusion coefficient, then the reciprocal of the measured confinement time is just the sum of the reciprocals of the individual confinement times associated with the individual diffusion coefficients. Since the individual processes probably scale in different ways, different ones may dominate under different circumstances. Evidence that this is indeed the case is found in the deterioration of confinement with the increase in MHD activity shown in Fig. 9. Note that the deterioration in confinement was more pronounced in H_e^4 plasmas, where the no-MHD confinement time was significantly longer than in the deuterium plasmas. This may be made more quantitative by assuming that the He^4 data in Fig. 9 result from two processes: one

whose characteristic confinement time (τ_{MHD}) depends only upon the MHD fluctuation level; the other which is independent of ΔB, but has the dependences represented by Eq. 5. A fit to the data yields $\tau_{MHD} \propto (\Delta B)^{-4}$, and is shown as the dashed line in Fig. 9. The behavior for injections into deuterium plasmas may then be determined by using the same $\tau_{MHD}(\Delta B)$, and is shown as the solid line in Fig. 9, in reasonable agreement with the data.

Allowing the possibility of different transport mechanisms with different dependences, it is remarkable that the impurity confinement times measured on six different tokamaks agree as well as they do with those predicted by Eq. 5. The general conclusion must be that the dominant impurity transport processes in all of these devices are similar, although the question of what microscopic mechanisms are responsible has not yet been answered.

7. Conclusions

The results of a set of experiments in which trace amounts of non-intrinsic impurities were injected into Alcator C plasmas have been described. The importance of a well known time history for the impurity source has been emphasized. The injected impurities were observed to penetrate quickly to the plasma center and then to leave gradually. The experimentally determined impurity emission time histories and silicon X-ray emission profiles have been compared with predictions of a computer code which models the impurity transport. The predictions of neoclassical transport are inconsistent with the empirical results. The assumption of transport by self-diffusion ($\Gamma_j \sim - \partial n_j/\partial r$) with a spatially uniform dif-

fusion coefficient (whose value depends upon the plasma parameters) leads to predictions consistent with the observations. From a purely practical point of view this means that, in ohmically heated tokamak plasmas which start out clean, impurities do not accumulate.

The particle confinement time was determined by monitoring the decay time of the central impurity emissions. The variations of this time with limiter safety factor, background ion mass, Z_{eff}, machine size, electron density, impurity charge and mass, and MHD fluctuation level were studied systematically. The empirical scaling results are provided in Eq. 5.

8. Acknowledgements

The authors would like to thank the entire Alcator Group. In particular, we acknowledge the contributions of R. Parker, B. Lipschultz and D. Gwinn for operation of the machine, R. Granetz for the MHD measurements and S. Kissel, R. Gandy and S. Wolfe for density and temperature measurements. For contributions to the design and operation of the soft X-ray diode array we thank especially R. Petrasso and N. Loter.

This work was supported by U.S. Department of Energy contracts DE-AC02-78ET51013 and DE-AC02-77ET53068.

REFERENCES

1. Hinnov, E., et al., Nucl. Fusion 18 (1978) 1305.
2. Fairfax, S. A., et al., in Plasma Physics and Controlled Nuclear Fusion Research (Proc. 8th Int. Conf. Brussels, 1980), Vol. 1, IAEA, Vienna (1981).
3. Cohen, S. A., Cecchi, J. L., Marmar, E. S., Phys. Rev. Lett. 35 (1975) 1507.
4. Marmar, E. S., Rice, J. E., Allen, S. L., Phys. Rev. Lett. 45 (1980) 2025.
5. TFR Group, Phys. Lett. 87A (1982) 169.
6. Burrell, K. H., et al., Nucl. Fusion 21 (1981) 1009.
7. Zhilinskil, A. P., et al., J.E.T.P. Lett. 32 (1980) 387.
8. Suckewer, S., et al., Phys. Lett. 80A (1980) 259.
9. Cohen, S., et al., J. Vac. Sci. Technol., 20 (1982) 1226.
10. Marmar, E., Cecchi, J., Cohen, S., Rev. Sci. Instrum. 46 (1975) 1149.
11. Engelhardt, W., et al., in Plasma Physics and Controlled Nuclear Fusion Research (Proc. 7th Int. Conf. Innsbruck, 1978) Vol. 1, IAEA, Vienna (1979) 123.
12. Isler, R. C., et al., Phys. Rev. Lett. 47 (1981) 333.
13. Marmar, E. S., Ph. D. Thesis, Princeton University, (1976) (unpublished).
14. Hawryluk, R. J., Suckewer, S., Hirshman, S. P., Nucl. Fusion 19 (1979) 607.
15. Seguin, F. H., Petrasso, R., Ann. Controlled Fusion Theory Conf. (1982), to be submitted to Phys. Rev. Lett. 1982.
16. Granetz, R. S., to be published in Phys. Rev. Lett. 1982.
17. Kissel, S. E., Sc.D. Thesis, Massachusetts Institute of Technology, (1982) (unpublished).
18. Lipschultz, B., et al., Bull. Am. Phys. Soc. 26 (1981) 975.
19. TFR Group, Phys. Rev. Lett. 36 (1976) 1306.

FIGURE CAPTIONS

Fig. 1: Comparison of impurity injections by (a) laser blowoff and (b) pulsed gas injection.

Fig. 2: Typical impurity injection into a hydrogen plasma. (For the density signal, 1 fringe = $.57 \times 10^{14} cm^{-3}$.)

Fig. 3: A detailed view (solid curves) of the normalized chordal brightnesses (with the backgrounds subtracted off) of sodium- (1394 Å), beryllium- (303 Å), helium- (6.65 Å) and hydrogen-like (6.18 Å) silicon as well as the central soft X-ray diode signal for injections into deuterium plasmas. The dashed curves are predictions from the computer model described in the text. Note that sawteeth are observeable on the Si^{13+} signal.

Fig. 4: The Abel-inverted soft X-ray silicon emission profiles (with the background subtracted off), for 5 different times after the injection, for a case similar to that shown in Fig. 2. The times shown are midway between internal disruptions.

Fig. 5: Code predictions for some of the traces of Fig. 3 using the neoclassical impurity flux of Eq. 2.

Fig. 6: Code predictions for the signals of Fig. 3 using the impurity flux of Eq. 3 with $d = 2.6 \times 10^3$ cm^2/sec. These curves are also shown as the dashed lines in Fig. 3 for a direct comparison with the observations.

Fig. 7. The observed chordal brightnesses (dots) of the soft X-ray silicon emission (non-inverted) as well as the code predictions (curves)

from Eq. 3, for a discharge similar to that shown in Fig. 3.

Fig. 8: Silicon confinement time as a function of electron density for hydrogen and deuterium discharges (a_L = 16 cm, 3.2 < q_L < 3.6).

Fig. 9: The impurity confinement time as a function of m = 2 amplitude for injections into helium and deuterium discharges.

Fig. 10: The impurity confinement time as a function of Z_{eff} for low density hydrogen discharges with 3.1 < q_L < 3.7 . Open circles represent discharges which did not exhibit sawtooth oscillations. The box represents ~ 100 injections into clean, higher density discharges.

Fig. 11: The impurity confinement times as a function of q_L^{-1} for aluminum, silicon and titanium injections into hydrogen, deuterium and helium plasmas with a_L = 16.5 cm.

Fig. 12: The impurity confinement time as a function of the charge of the injected impurity, for hydrogen discharges with a_L = 16.5 cm and 2.9 < q_L < 3.3.

Fig. 13: The silicon confinement time as a function of minor radius for hydrogen (3.1 < q_L < 4.2) and deuterium (3.1 < q_L < 3.6) discharges in Alcator C and Alcator A.

Fig. 14: The silicon confinement time as a function of major radius with a_L = 10 cm for hydrogen and deuterium discharges at constant q_L.

Fig. 15: The observed impurity confinement times as a function of those predicted by Eq. 5 for all Alcator C injections.

Fig. 16: The observed impurity confinement times as a function of those predicted by Eq. 5 for injections into Alcator A, TFR, FT-1, ISX-B and PDX. It should be noted that the observed times from PDX and ISX-B were obtained by fits to data in Figs. 2 and 1 from references 8 and 6, respectively, while in the other cases the values for the exponential decay times were provided.

a) laser blowoff

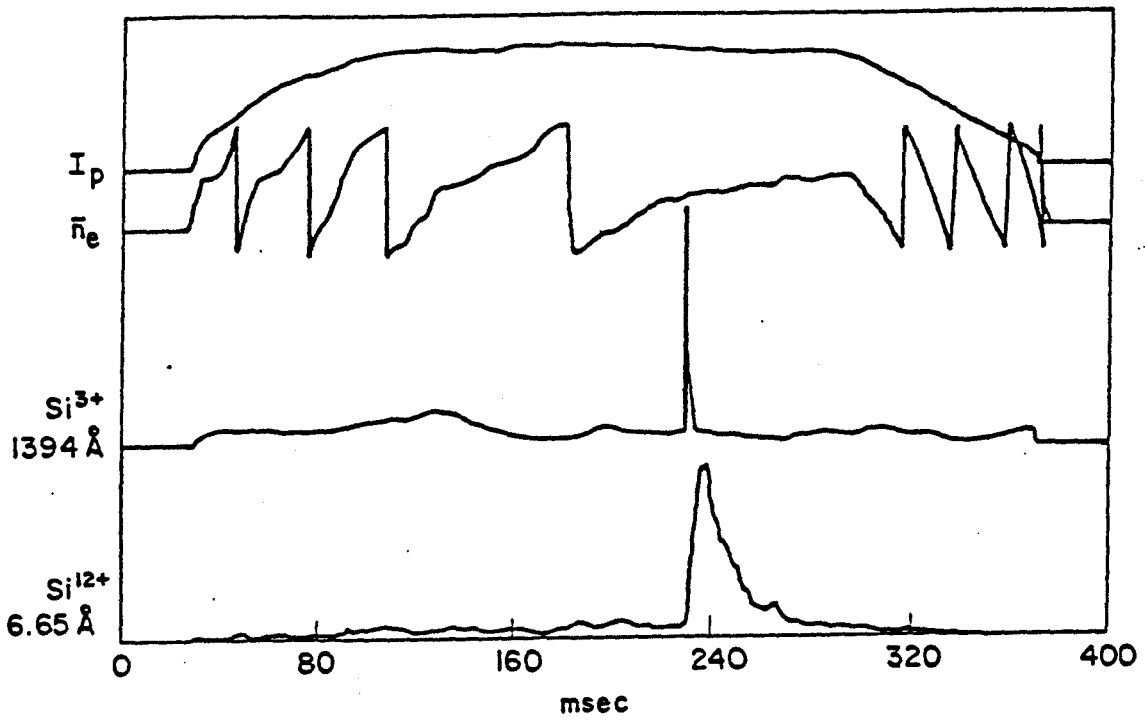

FIGURE 1A

b) gaseous injection

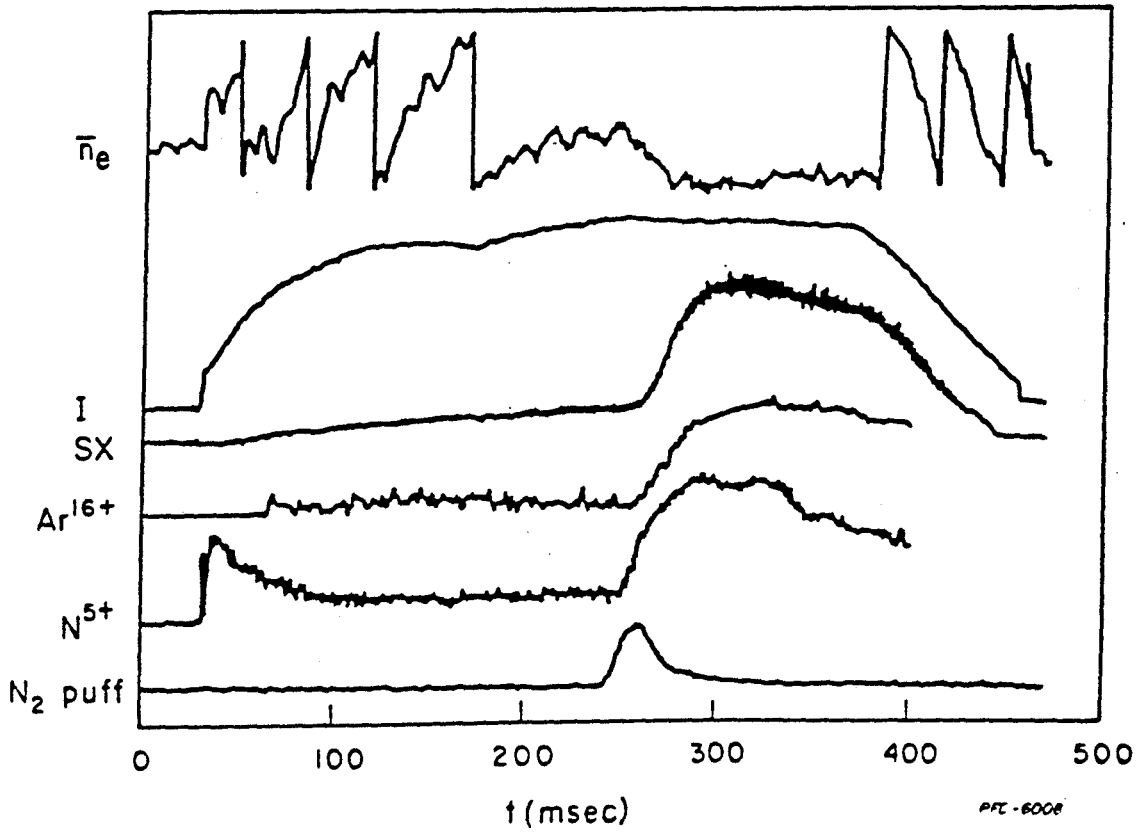

FIGURE 1B

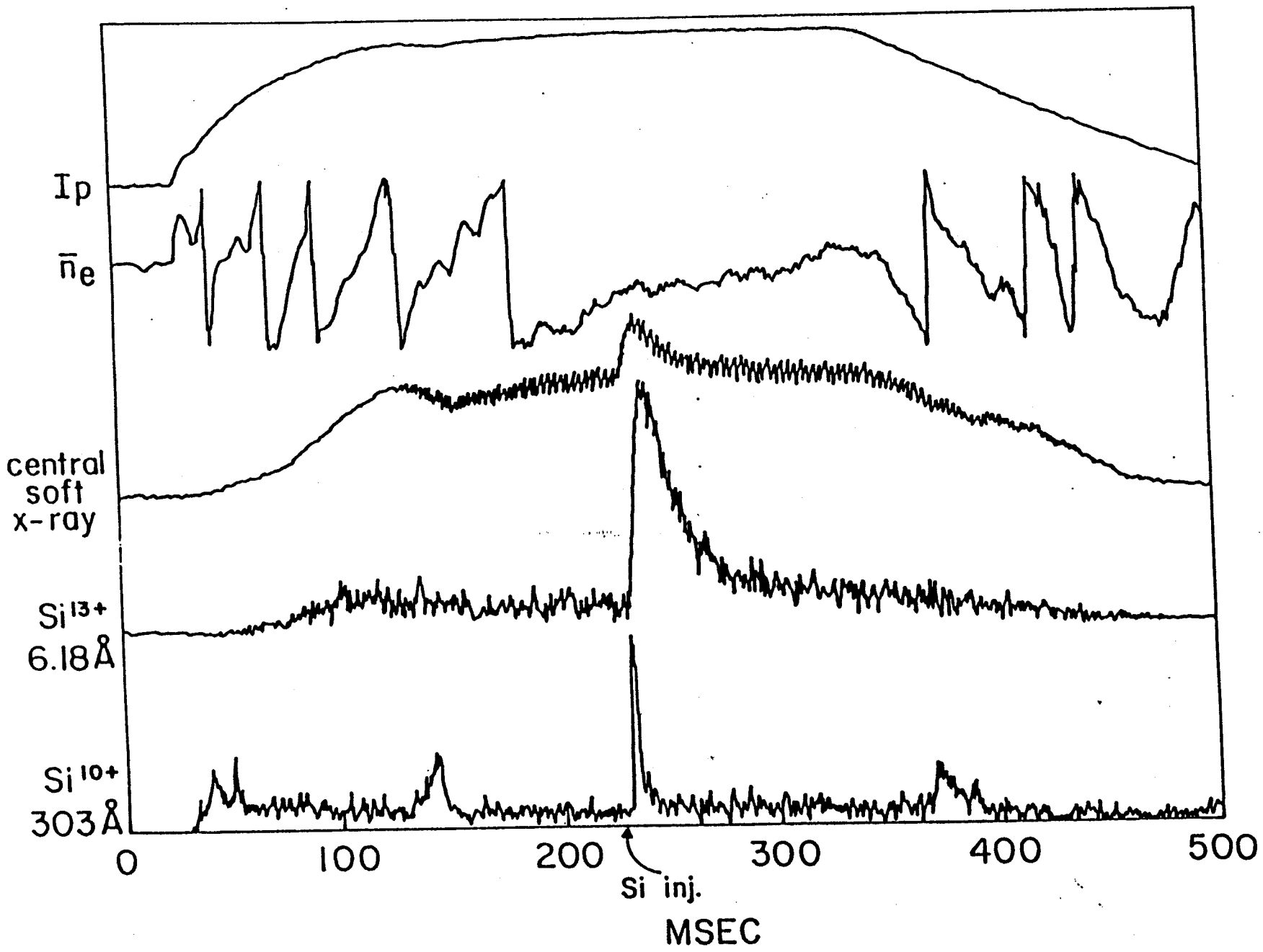
Ip
$\bar{n}_e$
central soft x-ray
Si^{13+} 6.18Å
Si^{10+} 303Å
0
100
200
300
400
500
Si inj.
MSEC

FIGURE 2

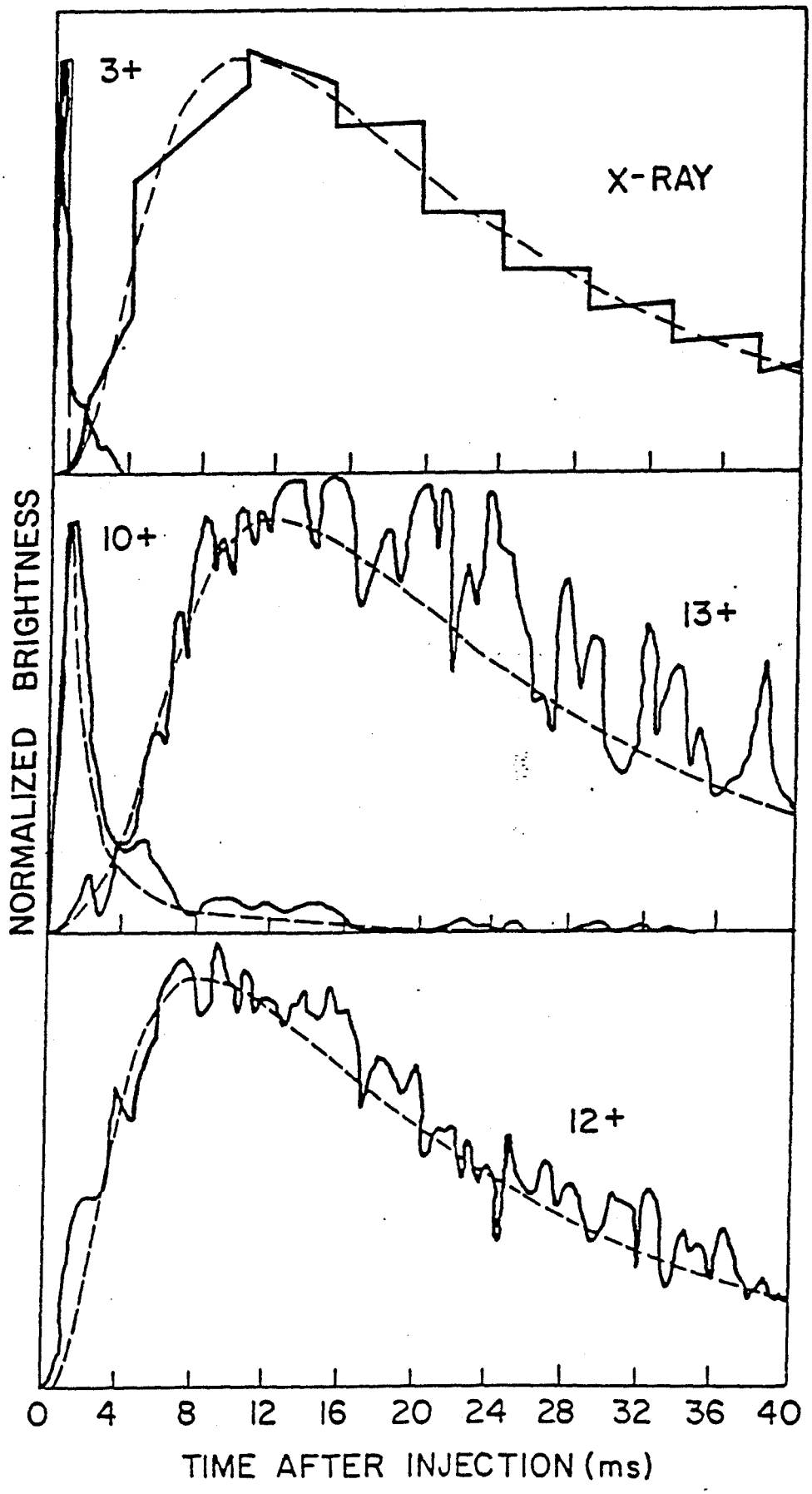

PFC-7092

FIGURE 3

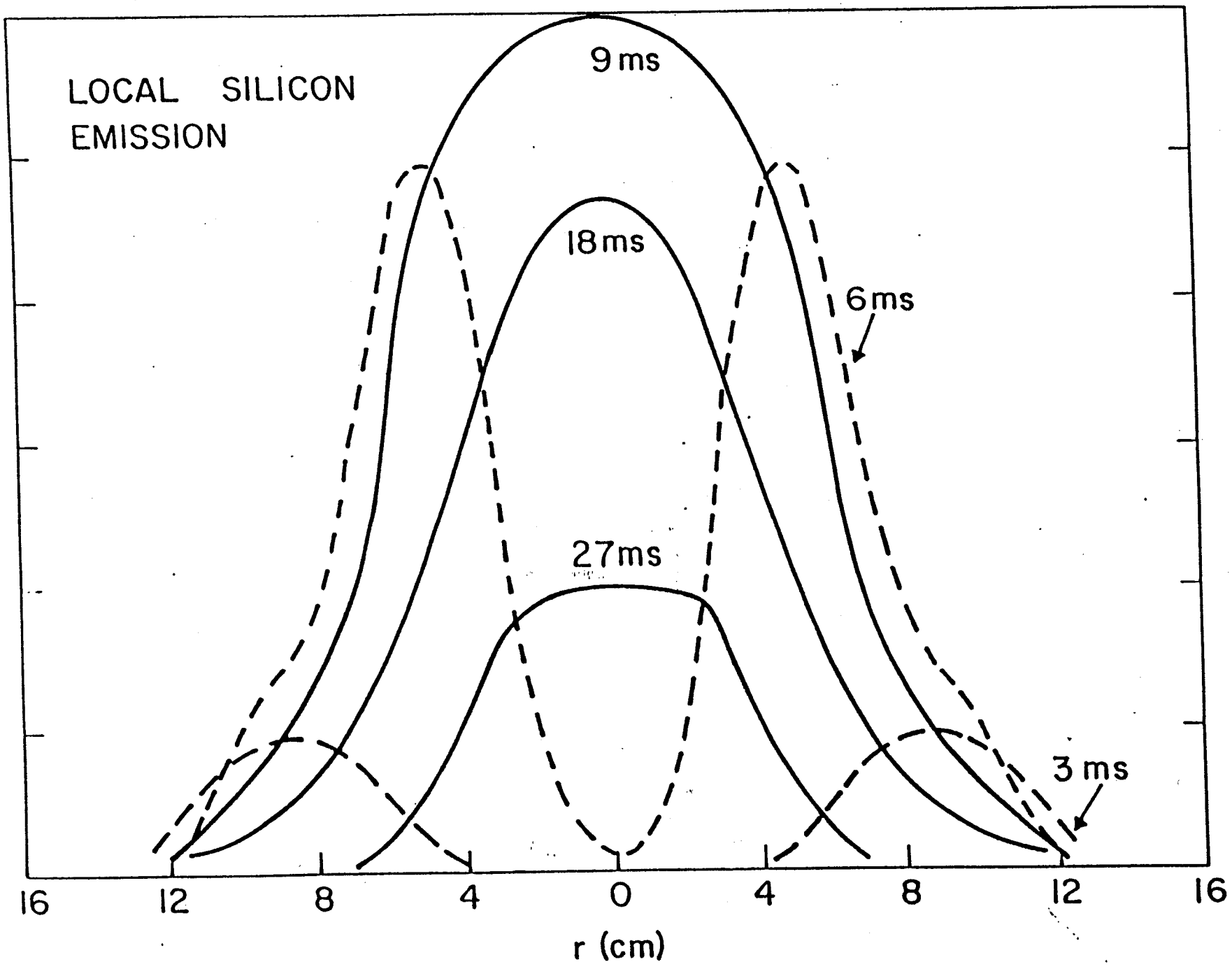
LOCAL SILICON
EMISSION
9ms
18ms
6ms
27ms
3ms
16
12
8
4
0
4
8
12
16
r (cm)
PFC-7032

FIGURE 4

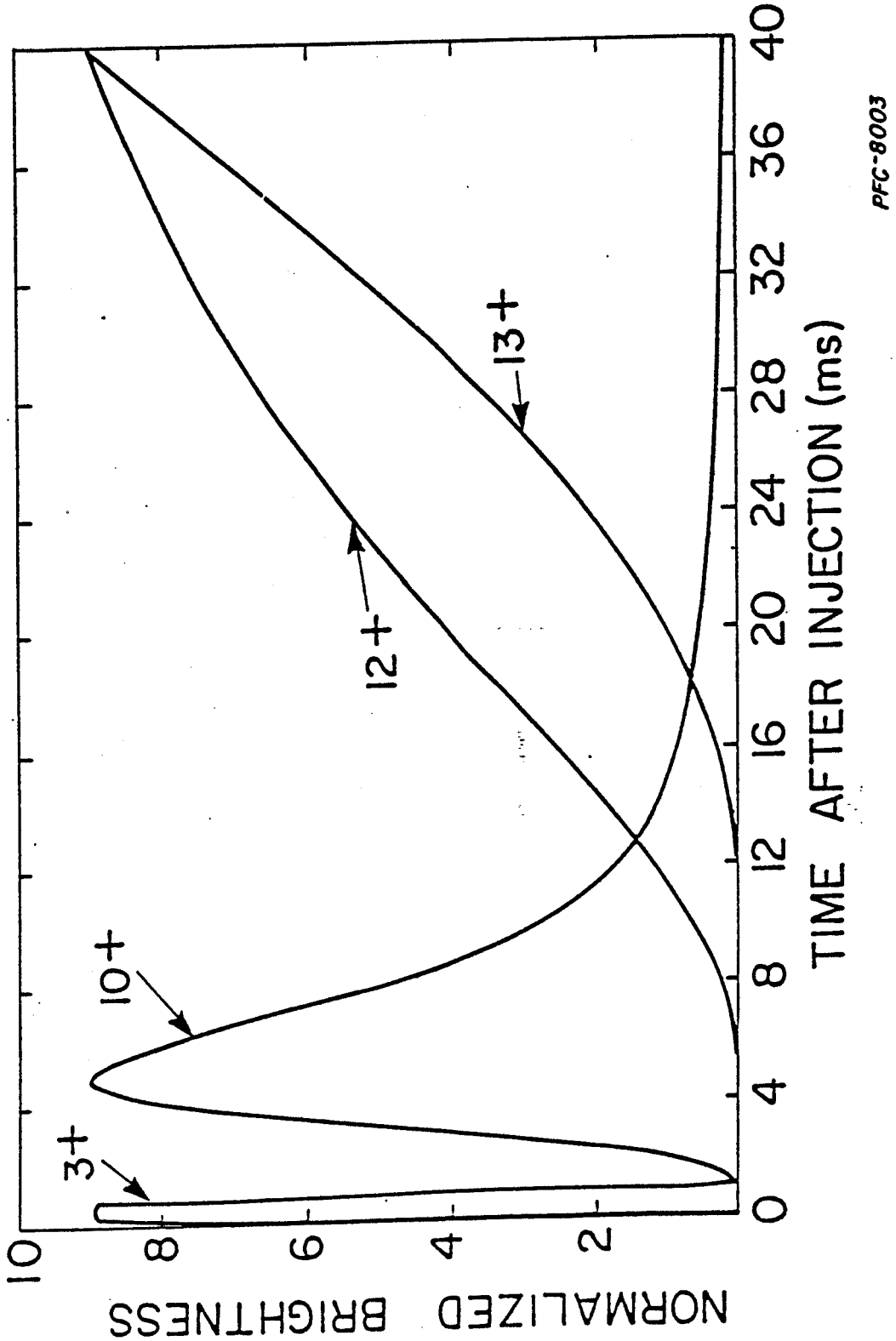
NORMALIZED BRIGHTNESS
10
8
6
4
2
0
4
8
12
16
20
24
28
32
36
40
TIME AFTER INJECTION (ms)
3+
10+
12+
13+
PFC-8003

FIGURE 5

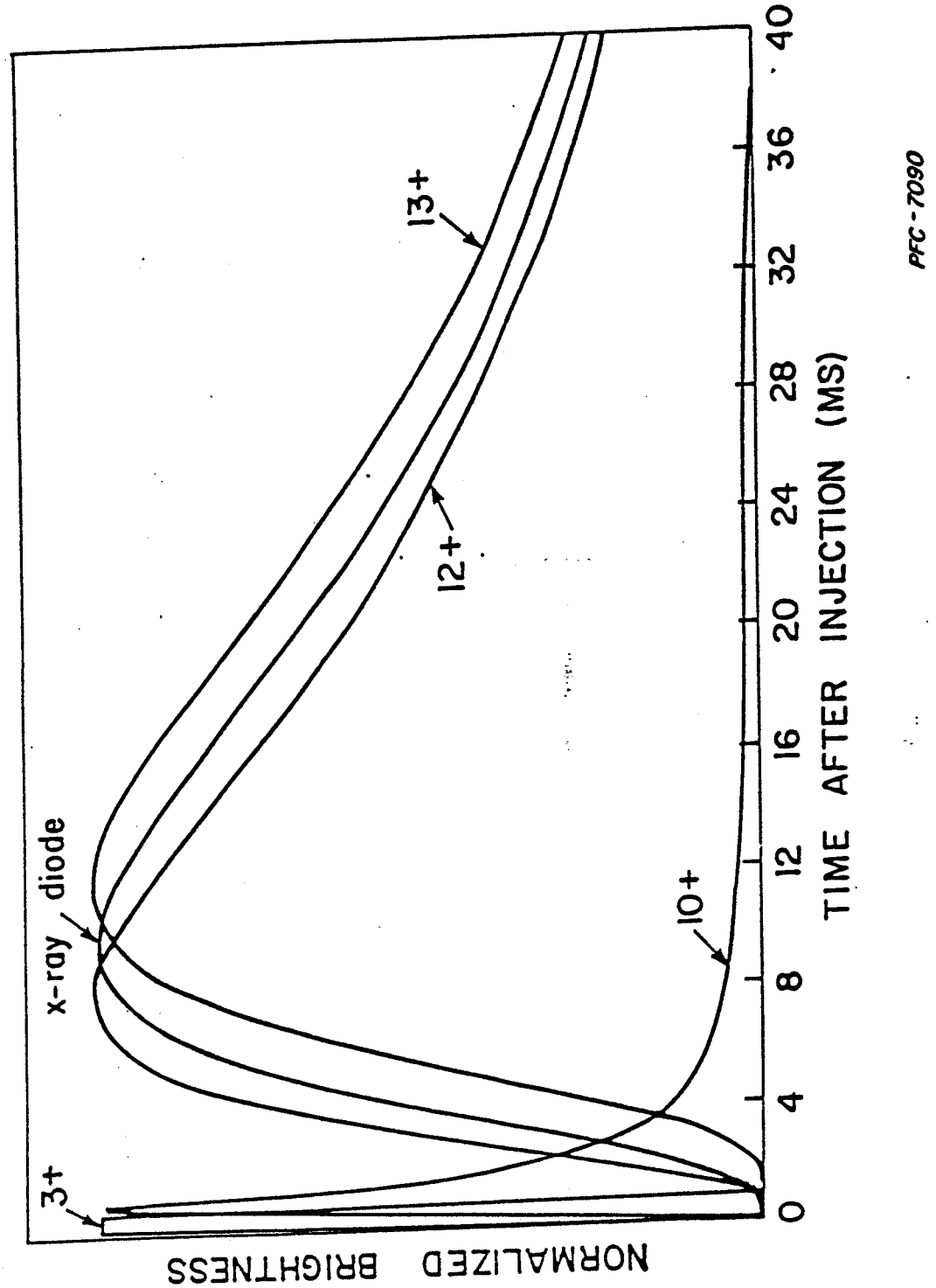
NORMALIZED BRIGHTNESS
TIME AFTER INJECTION (MS)
0
4
8
12
16
20
24
28
32
36
40
3+
x-ray diode
10+
12+
13+
PFC-7090

FIGURE 6

X-RAY BRIGHTNESS PROFILES

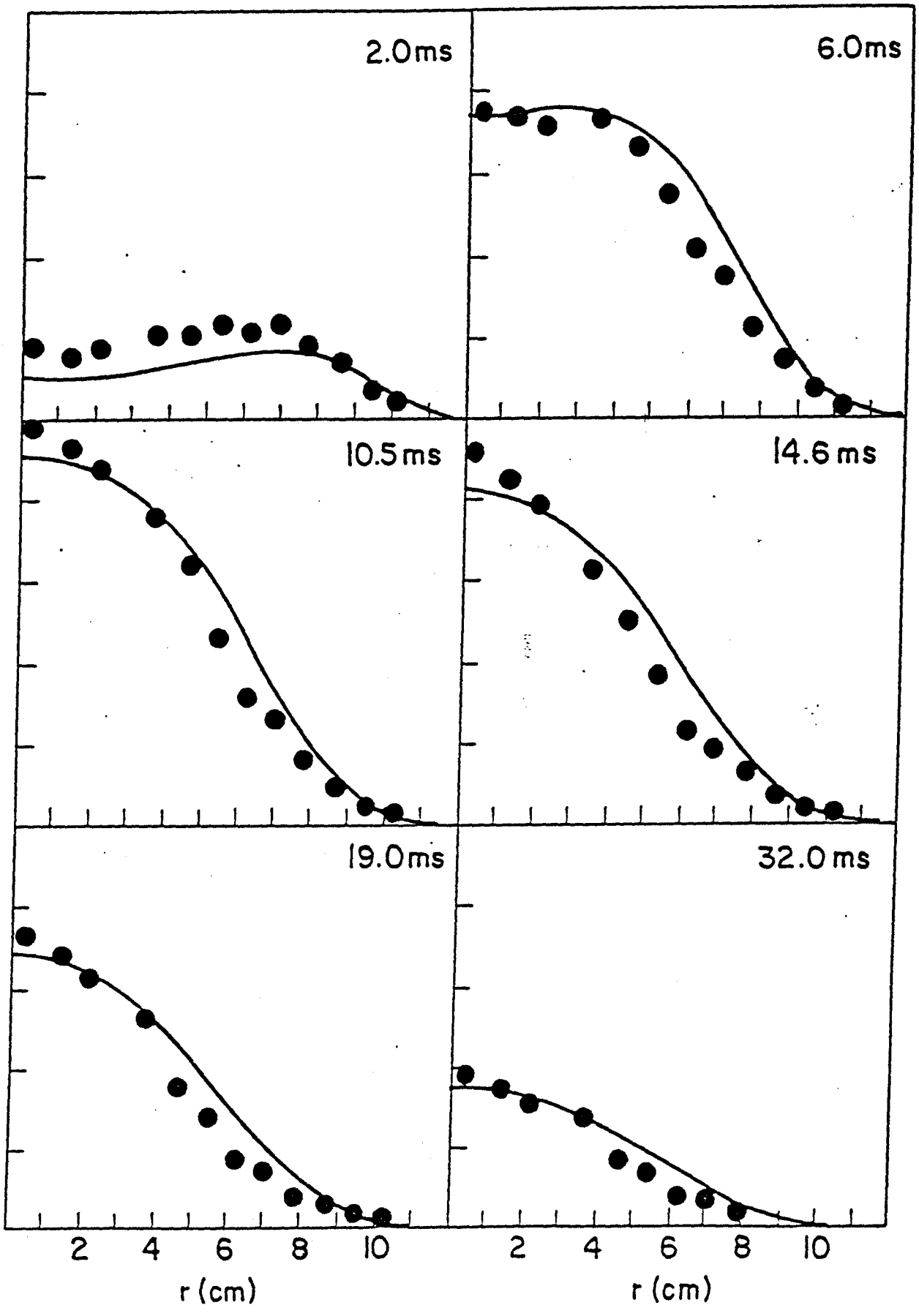

FIGURE 7

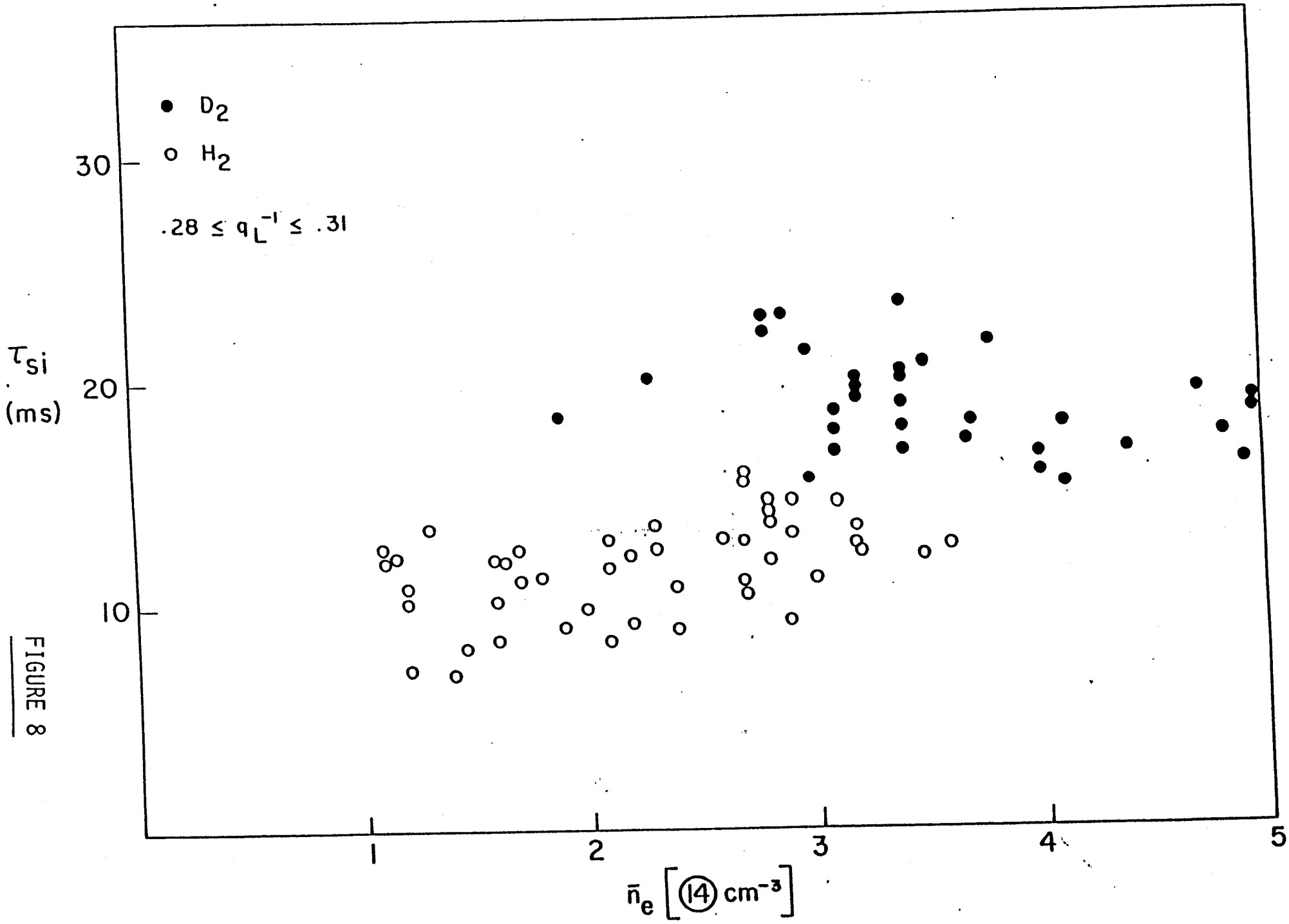

FIGURE 8

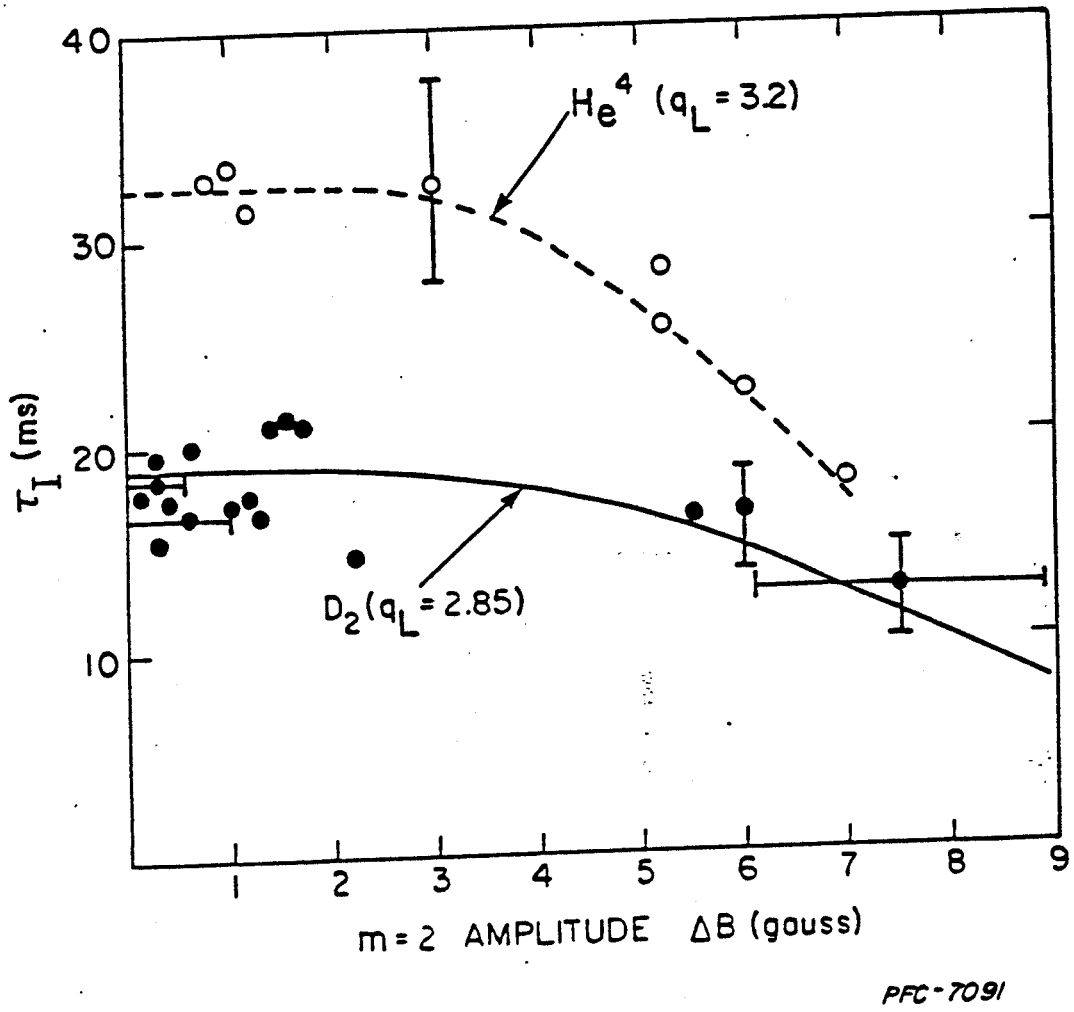
40
30
20
10
τ_I (ms)
He^4 (q_L = 3.2)
D_2 (q_L = 2.85)
1
2
3
4
5
6
7
8
9
m = 2 AMPLITUDE ΔB (gauss)
PFC-7091

FIGURE 9

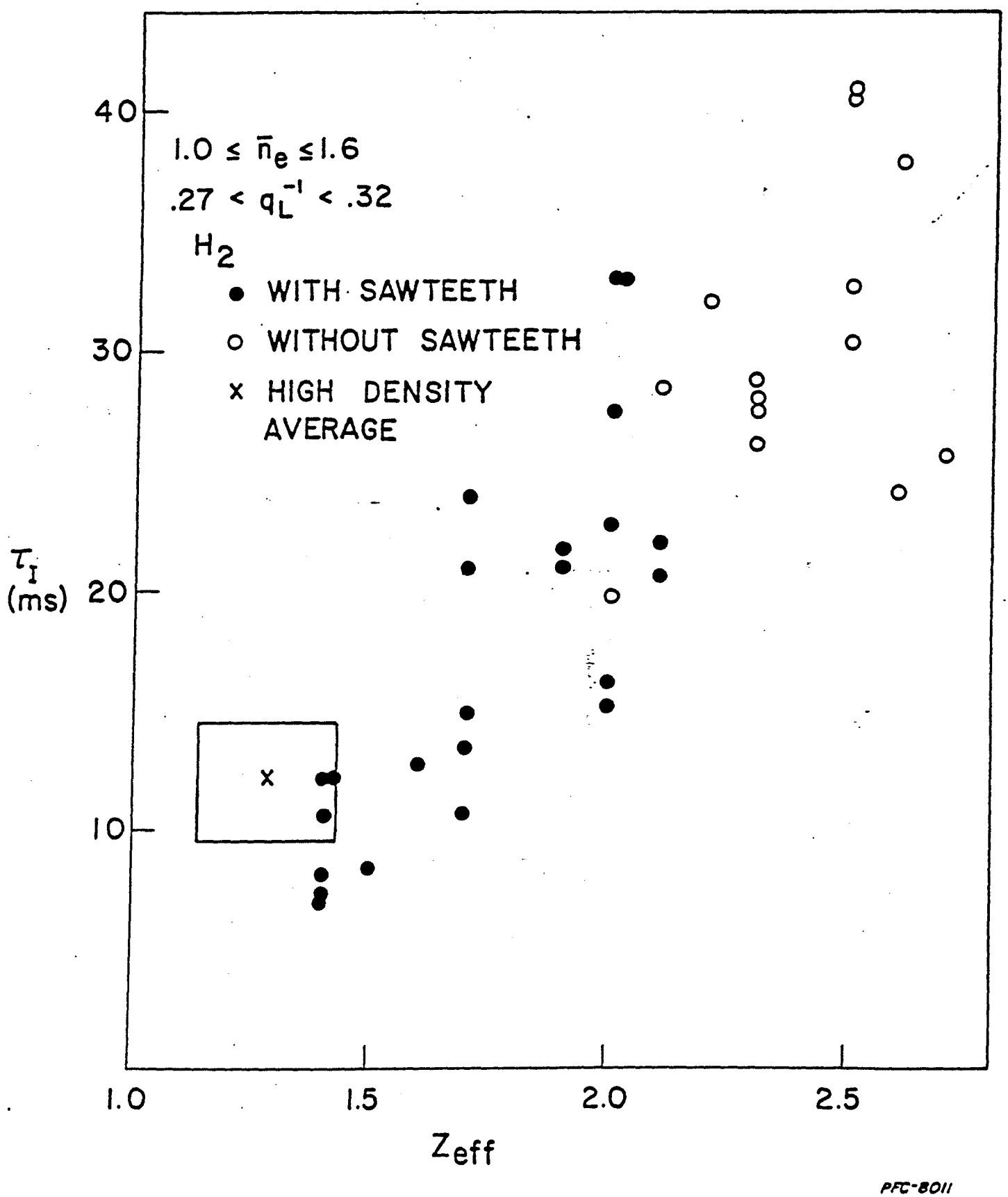
40
30
20
10
τ_I (ms)
$1.0 \leq \bar{n}_e \leq 1.6$
$.27 < q_L^{-1} < .32$
H_2
WITH SAWTEETH
WITHOUT SAWTEETH
HIGH DENSITY AVERAGE
8
x
1.0
1.5
2.0
2.5
Z_{eff}
PFC-8011

FIGURE 10

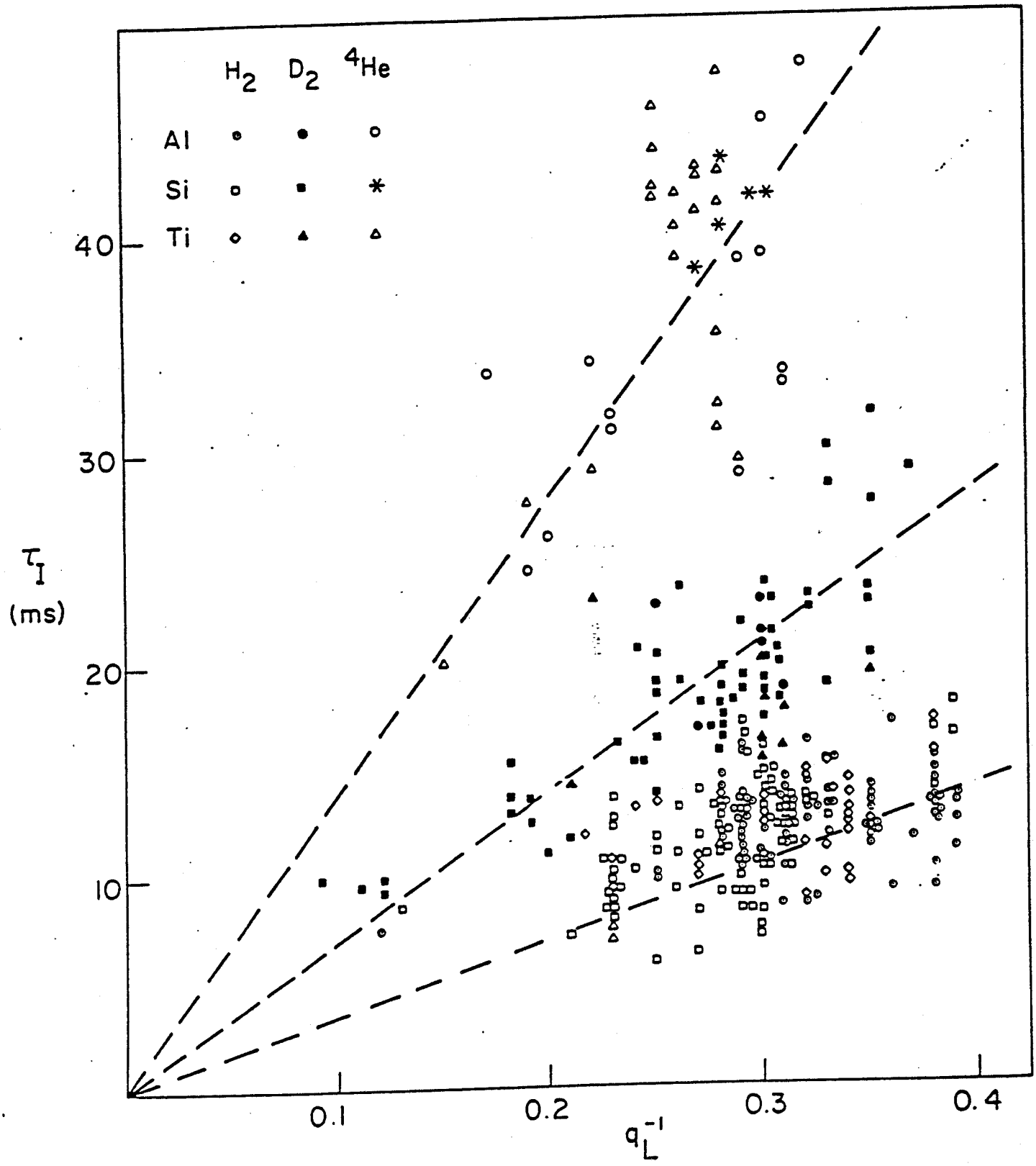

FIGURE 11

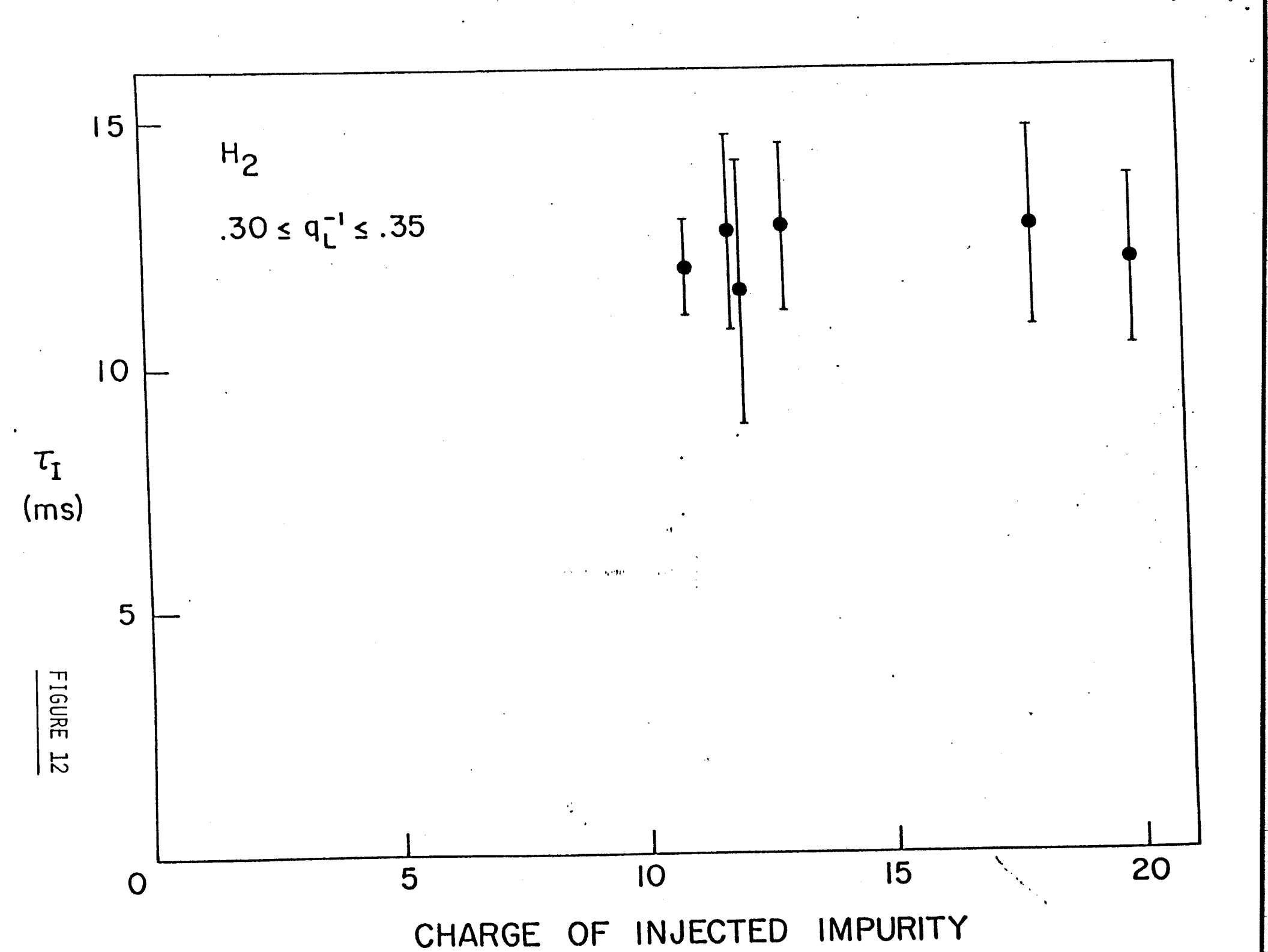
15
10
5
0
H_2
$.30 \leq q_L^{-1} \leq .35$
τ_I
(ms)
5
10
15
20
CHARGE OF INJECTED IMPURITY

FIGURE 12

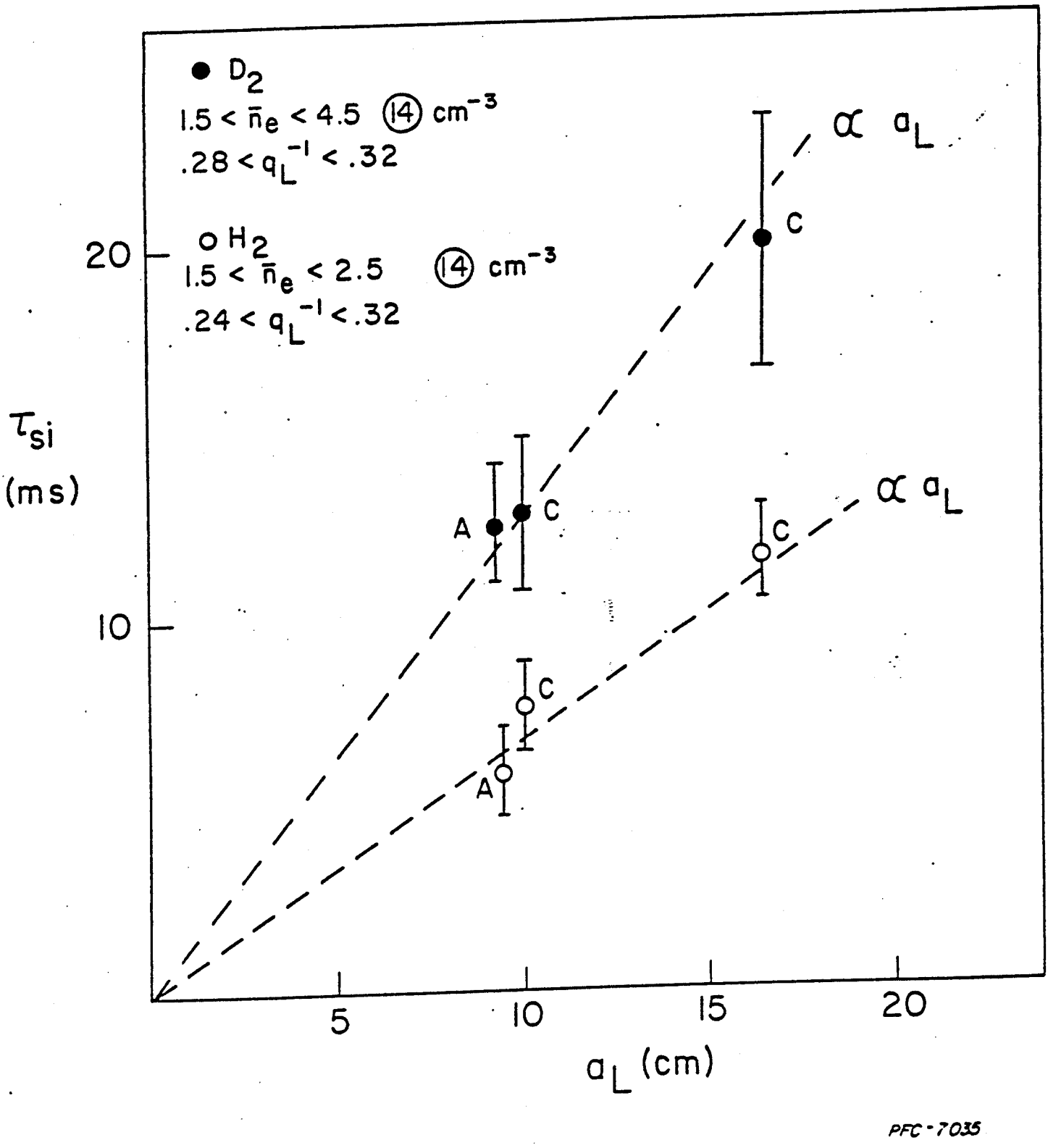
● D_2
$1.5 < \bar{n}_e < 4.5$ (14) cm^{-3}
$.28 < q_L^{-1} < .32$
○ H_2
$1.5 < \bar{n}_e < 2.5$ (14) cm^{-3}
$.24 < q_L^{-1} < .32$
$\alpha\ a_L$
$\alpha\ a_L$
A
C
C
C
C
A
20
10
τ_{si} (ms)
5
10
15
20
a_L (cm)
PFC-7035

FIGURE 13

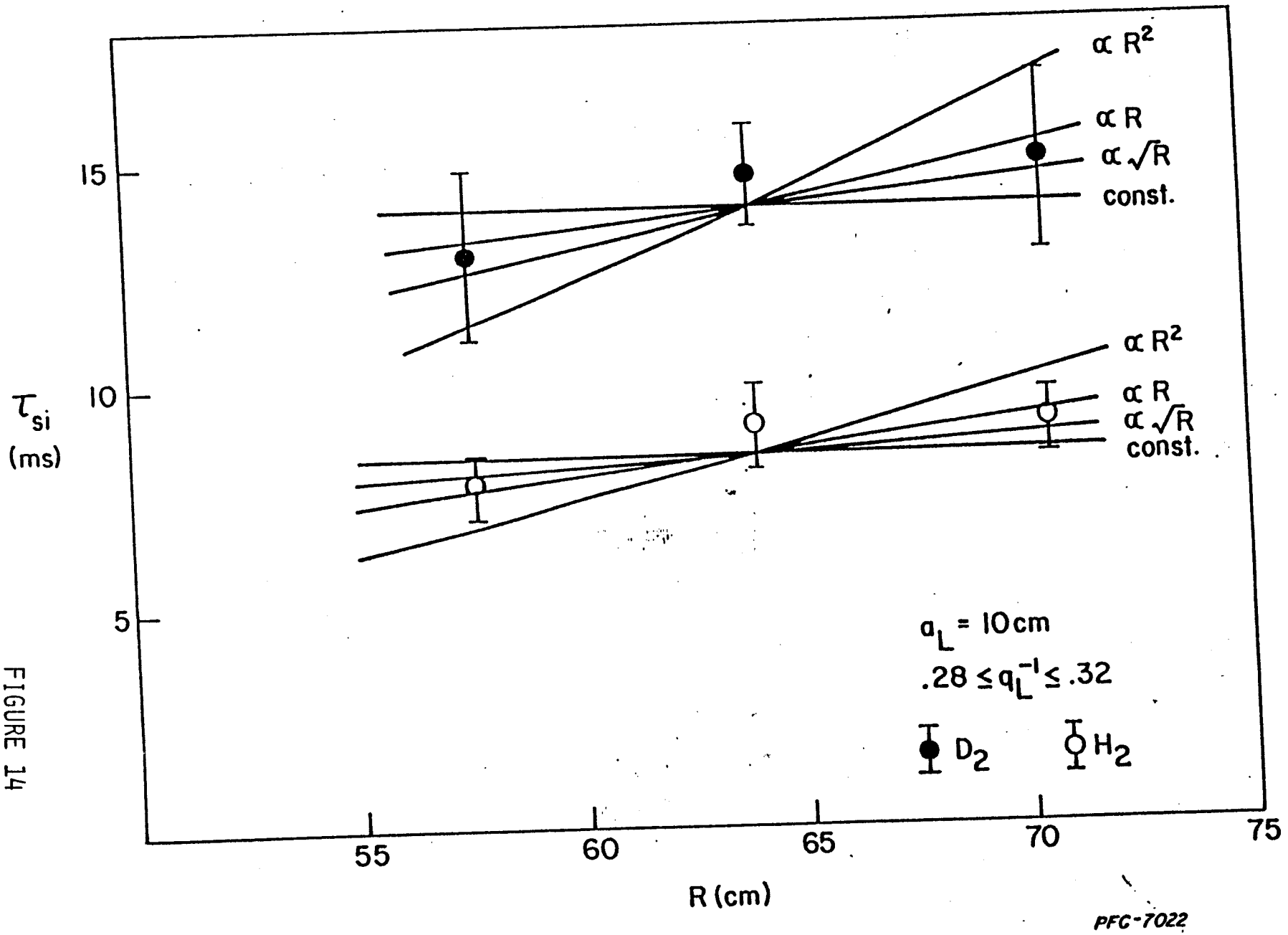
15
10
5
τ_{si} (ms)
55
60
65
70
75
R (cm)
$\propto R^2$
$\propto R$
$\propto \sqrt{R}$
const.
$\propto R^2$
$\propto R$
$\propto \sqrt{R}$
const.
$a_L = 10\,cm$
$.28 \leq q_L^{-1} \leq .32$
D_2
H_2
PFC-7022

FIGURE 14

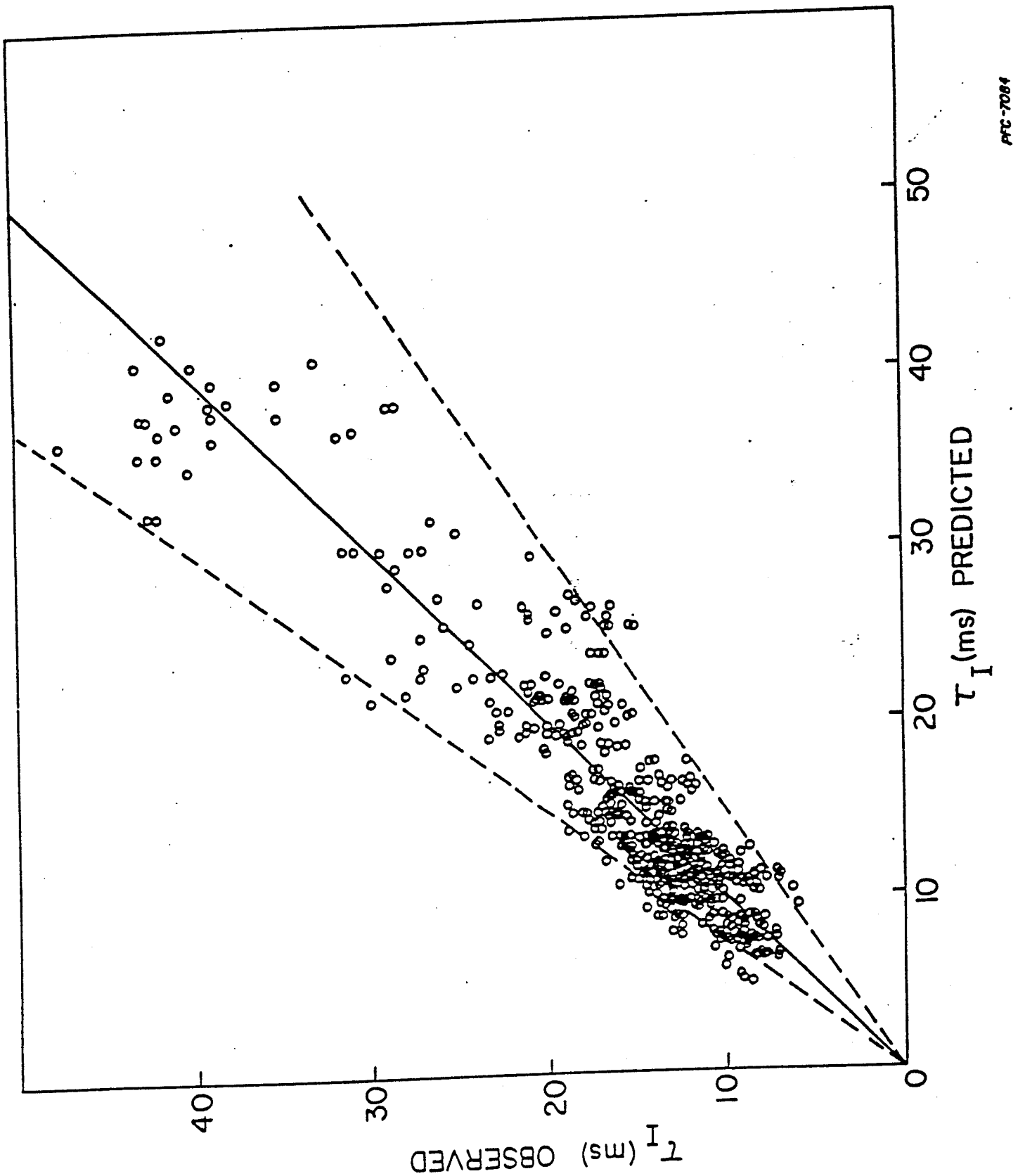

FIGURE 15

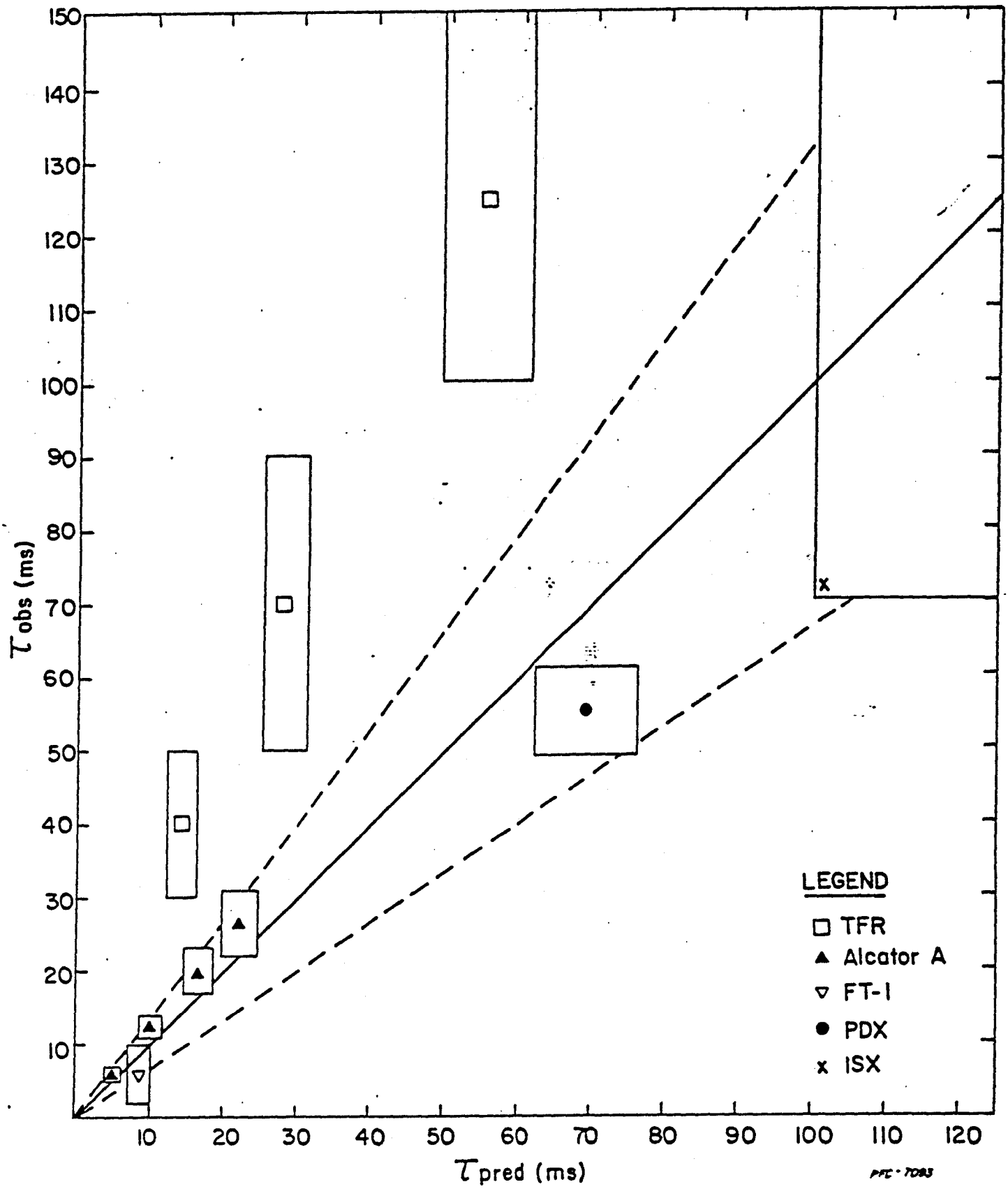
150
140
130
120
110
100
90
80
70
60
50
40
30
20
10
τ obs (ms)
10
20
30
40
50
60
70
80
90
100
110
120
τ pred (ms)
LEGEND
TFR
Alcator A
FT-1
PDX
ISX
PFC-7083

FIGURE 16